Deep Learning the Morphology of Dark Matter Substructure

Stephon Alexander, Evan McDonough
Department of Physics, Brown University
Brown Theoretical Physics Center, Brown University

Sergei Gleyzer
Department of Physics and Astronomy, University of Alabama

Michael W. Toomey[*], **Emanuele Usai**
Department of Physics, Brown University

Abstract

Strong gravitational lensing is a promising probe of the substructure of dark matter halos. Deep learning methods have the potential to accurately identify images containing substructure, and differentiate particle dark matter from other well motivated theories, including vortex substructure of dark matter condensates and superfluids. We implement a classification approach to identifying dark matter based on simulated strong lensing images with different substructure. Utilizing convolutional neural networks trained on sets of simulated images, we demonstrate the feasibility of deep neural networks to reliably distinguish among different types of dark matter substructure. With thousands of strong lensing images anticipated with the coming launch of Large Synoptic Survey Telescope (LSST), we expect that supervised and unsupervised deep learning models will play a crucial role in determining the nature of dark matter.

1 Introduction

The canonical candidate for dark matter is a weakly interacting massive particle (WIMP). However, WIMPS have thus far evaded detection, both by direct detection [1, 2, 3, 4, 5] and colliders (e.g. [6]). There are also hints at cracks in the WIMP paradigm, for example, the core vs. cusp problem. This motivates the consideration of alternatives to the WIMP paradigm.

An interesting possibility is *condensate* models of dark matter, both Bose-Einstein (BEC) [7, 8, 9, 10, 11, 12, 13] and Bardeen-Cooper-Schreifer (BCS) [14, 15]. In these models, dark matter is a quasi-particle excitation of the fundamental degrees of freedom that comprise the condensate. These models have the interesting property that they can form *vortices* [16], line-like defects that are a non–relativistic analog to cosmic strings [17, 18]. The detection of vortices would be a smoking gun for superfluid dark matter.

If they exist, vortices constitute a substructure component for dark matter halos. In practice, the best method to detect substructure is from strong gravitational lensing images [19, 20, 21, 22, 23, 24, 25]. In this work we take a new approach, and with condensate models of dark matter in mind, implement a deep learning algorithm to identify specific types of dark matter in simulated lensing images; that is, we consider the search for substructure as a classification problem.

[*]michael_toomey@brown.edu

33rd Conference on Neural Information Processing Systems (NeurIPS 2019), Vancouver, Canada.

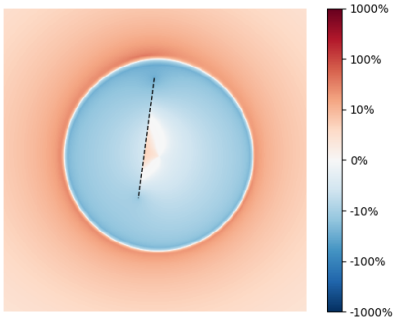

Figure 1: Residuals image with superfluid substructure (a vortex).

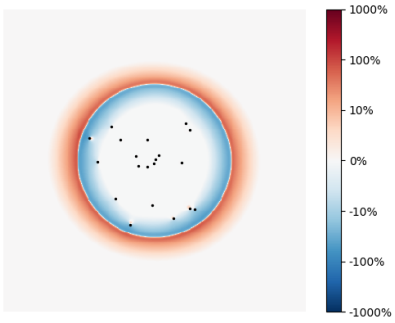

Figure 2: Same as Figure 1 but for particle substructure.

1.1 Dark Matter Substructure and Gravitational Lensing

The, Lambda cold dark matter, ΛCDM paradigm predicts that density fluctuations present in the the early universe evolve to become the large scale structure of the universe via hierarchical structure formation. This model envisions small halos merge together forming larger and larger structures leading to the dark matter halos that we see today [26].

A powerful probe of the gravitationally bound structures of dark matter is strong gravitational lensing. Given a matter over or under density, the deflection angle along the line of sight is given by an integral over the induced gravitational potential. The gravitational potential is in turn determined by matter density via the Poisson equation, $\nabla^2\Psi \propto \rho$. The linearity of this equation implies that the total lensing due to the separate contributions, e.g. of a halo and halo substructure, is simply the sum of the individual contributions.

Lensing is well-studied due to the spherical substructures expected from hierarchical structure formation in the context of non-interacting particle dark matter. However, other types of substructure can exist in models of dark matter outside the WIMP paradigm. As a prototypical example, we will consider dark matter condensates, namely superfluids, which exhibit substructure in the form of *vortices*. Solutions describing vortices in dark matter halos were found in [27].

The vortex solution is characterized by a density profile that can be parameterized by a core-radius r_v and scaling exponent, which effectively models the vortex as a tube. On distance scales much larger then r_v, the vortex can be approximated as a line. The values of these parameters: the density and total mass of the vortices, as well as the expected number density in realistic dark matter halos, varies widely across the literature.

1.2 Strong Lensing Images

At this moment strong lensing data is limited to a handful of images. However, the upcoming completion of the Large Synoptic Survey Telescope (LSST) will lead to thousands of strong lensing images that can be analyzed [28]. In this work we have chosen to simulate our lensing images using the package *PyAutoLens* [29, 30]. Written in Python, it can produce a variety of simulated strong lensing images where the user can adjust, among many possibilities, the mass of the halo, include substructure, light profiles, and mass profiles.

In addition to the simulation of the lensing itself, we also consider the addition of noise and the modifications induced by a point spread function (PSF) on our observation. Thus, we can vary the level of noise in our images and include a PSF that is in line with real world instruments like Hubble or the future LSST, in this case both sub–arcsecond resolution. Following [31], we approximate the PSF as an Airy disk whose first zero-crossing occurs at a radius of $\sigma_{psf} <$ arcsec. This approximation is valid when noise is dominated by diffraction, which we assume to be the case.

The residual lensing image (the lensing image from a halo without substructure subtracted from one with substructure) due to a single vortex embedded in a halo, with the vortex mass 1% that of the

Table 1: Parameters with distributions and priors used in the simulation of strong lensing images. Where two values are given, the first corresponds to our Modal A and the second Model B. Note that only a single type of substructure was used per image.

Lensing Galaxy – *Sersic Light Profile*			
Parameter	**Distribution**	**Priors**	**Details**
θ_x	fixed	0	x position
θ_y	fixed	0	y position
z	fixed | uniform	0.5 | [0.4,0.6]	redshift
e	uniform	[0.5, 1.0]	axis ratio
ϕ	uniform	[0, 2π]	orientation relative to y axis
I	fixed	1.2	intensity of emission (arbitrary units)
n	fixed	2.5	Sersic index
R	fixed | uniform	0.5 | [0.5,2]	effective radius
Dark Matter Halo – *Spherical Isothermal*			
Parameter	**Distribution**	**Priors**	**Details**
θ_x	fixed	0	x position
θ_y	fixed	0	y position
θ_E	fixed	1.2	Einstein radius
External Shear			
Parameter	**Distribution**	**Priors**	**Details**
γ_{ext}	uniform	[0.0, 0.3]	magnitude
ϕ_{ext}	uniform	[0, 2π]	angle
Lensed Galaxy – *Sersic Profile*			
Parameter	**Distribution**	**Priors**	**Details**
r	uniform	[0, 1.2]	radial distance from center
ϕ_{bk}	uniform	[0, 2π]	angular position of galaxy from y axis
z	fixed | uniform	1.0 | [0.8,1.2]	redshift
e	uniform	[0.7, 1.0]	axis ratio
ϕ	uniform	[0, 2π]	orientation relative to y axis
I	uniform	[0.7, 0.9]	intensity of emission (arbitrary units)
n	fixed	1.5	Sersic index
R	fixed	0.5	effective radius
Vortex			
Parameter	**Distribution**	**Priors**	**Details**
θ_x	fixed | normal	0 | $[0.0, 0.5]$	x position
θ_y	fixed | normal	0 | $[0.0, 0.5]$	y position
l	fixed | uniform	1.0 | [0.5,2.0]	length of vortex
ϕ_v	uniform	[0, 2π]	orientation from y axis
m_{vort}	fixed	0.01 M_{Halo}	total mass of vortex
Spherical			
Parameter	**Distribution**	**Priors**	**Details**
r	uniform	[0, 1.0]	radial distance from center
ϕ_{sph}	uniform	[0, 2π]	angular position of galaxy from y axis
N	fixed | Poisson	25 | μ=25	number of substructures
m_{sub}	fixed	0.01 M_{Halo}	total mass of subhalos

halo, is shown in Figure 1. We do the same for spherical substructure, as studied in [31], in Figure 2. From these images one can appreciate the difference in lensing is primarily in the the *morphology* of the signal, making this an ideal task for a classification with a convolutional neural network.

Lensing images used in our analysis were generated with standard astrophysical parameters, given in Table 1. We have included the light from the lensing galaxy and non–negligible backgrounds and noise. We have also accounted for other instrumental effects like the point spread function which we have modeled after the expected resolution of LSST, as well as shear effects.

In addition to the vortex and spherical sub-halo substructure classes discussed previously, there remains the possibility that an image may not have any detectable substructure at all, e.g. if the Einstein radius of the substructure is predominantly smaller then the PSF of the detector. Given this, we introduce an additional class: no substructure present.

2 Network & Training

We evaluate a set of convolutional neural networks to identify different types of dark matter substructure, using ResNet18 [32], AlexNet [33], DenseNet [34], and VGG [35], and choose ResNet18, as its defining feature is that residual networks can skip layers all together in training, speeding up the learning rate. During training we make use of data augmentation (see e.g. [33]) via translation and rotations up to 90°. These all constitute invariant transformations with respect to the

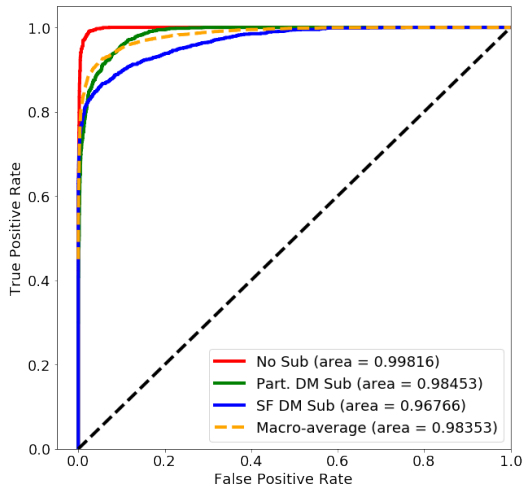

Figure 3: ROC curve for multiclass substructure classification with *ResNet18*.

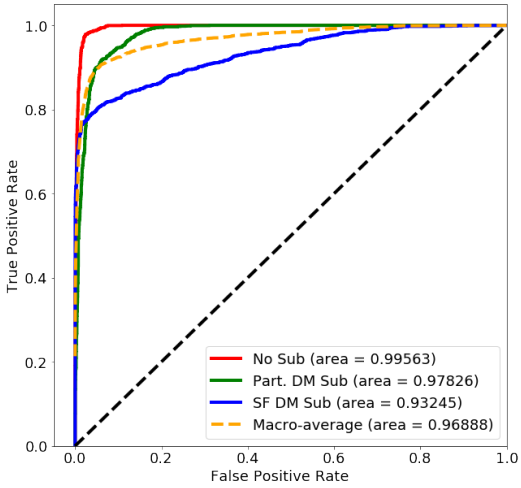

Figure 4: Same as Figure 3 but including more variations across population of images.

underlying substructure that allow the network to learn the actual structure in images. We utilize 150,000 training and 15,000 validation images. The binary cross–entropy loss was minimized with the Adam optimizer in batches of 200 over a total of at most 20 epochs. The learning rate starts with a value of 1×10^{-4} and is reduced by a factor of ten when the validation loss is not improved for 3 consecutive epochs. The networks were implemented using the PyTorch package and run on a single NVIDIA Titan K80 GPU.

3 Results

A multi–class classifier was trained to predict the three classes: vortex, spherical, and no-substructure. Three additional binary classifiers were then trained to distinguish between the two most probable classes predicted by the multi-class classifier. All classifiers were trained using realistic mock lensing images as described previously, with parameters given in Table 1.

The AUC scores for substructure classification by ResNet18 were 0.998, 0.985, and 0.967, for images with no substructure, spherical sub-halos, and vortices, respectively, see Figure 3. After allowing for additional image variations, so as to model a diverse set of physical systems, we obtain AUC scores of 0.996, 0.978, and 0.932, see Figure 4. Specifically, we vary the distance to the lensing and lensed galaxy, the galaxy size, and importantly, the intensity of the background and noise, allowing the background to become non-negligible. We also vary the position of the vortex, and for spherical substructure consider the number of halos to be taken from a Poisson draw with mean 25. The details of all parameters are included in Table 1. Our results indicate that our algorithm achieves excellent performance in the classification of dark matter substructure, including in the presence of additional degrees of freedom.

To complete the analysis of this work, we establish the detection threshold for our network by changing the total mass of the substructure while holding all other parameters constant. We implement this by simulating sets of 50,000 training and 5,000 validation images at different total fractions of the halo mass.

We find that the AUC rapidly deteriorates for a substructure mass below $10^{-2.5} \approx 0.3\%$ of the halo mass. From this we conclude that a convolutional network, given fixed computing resources, can reliably identify lensing images containing substructure, provided that it constitutes at least a fraction of a percent of the dark matter in the halo.

4 Discussion & Conclusion

It is well established that substructure can constrain dark matter models. In this work we demonstrate the feasibility of learning the morphology of dark matter subtructure in strong lensing images. Utilizing a supervised convolutional neural network, trained on simulated images, we have demonstrated that it is possible for a model to reliably distinguish among different types of dark matter substructure. Finally, we note that deep learning may be amenable to searching for dark matter vortices in other observational windows, analogous to searches for cosmic strings in the cosmic microwave background.

Acknowledgments

The authors thank Cora Dvorkin, Javad Hashemi, Shirley Ho, and David Spergel, for useful discussions. One of the authors thanks Robert Brandenberger for encouragement to work on this topic more than 20 years ago.

References

[1] A. K. Drukier, Katherine Freese, and D. N. Spergel. Detecting Cold Dark Matter Candidates. *Phys. Rev.*, D33:3495–3508, 1986.

[2] Mark W. Goodman and Edward Witten. Detectability of Certain Dark Matter Candidates. *Phys. Rev.*, D31:3059, 1985. [,325(1984)].

[3] D. S. Akerib et al. Results from a search for dark matter in the complete LUX exposure. *Phys. Rev. Lett.*, 118(2):021303, 2017.

[4] Xiangyi Cui et al. Dark Matter Results From 54-Ton-Day Exposure of PandaX-II Experiment. *Phys. Rev. Lett.*, 119(18):181302, 2017.

[5] E. Aprile et al. Dark Matter Search Results from a One Ton-Year Exposure of XENON1T. *Phys. Rev. Lett.*, 121(11):111302, 2018.

[6] Morad Aaboud et al. Constraints on mediator-based dark matter and scalar dark energy models using $\sqrt{s} = 13$ TeV pp collision data collected by the ATLAS detector. *JHEP*, 05:142, 2019.

[7] Sang-Jin Sin. Late time cosmological phase transition and galactic halo as Bose liquid. *Phys. Rev.*, D50:3650–3654, 1994.

[8] M. P. Silverman and Ronald L. Mallett. Dark matter as a cosmic Bose-Einstein condensate and possible superfluid. *Gen. Rel. Grav.*, 34:633–649, 2002.

[9] Wayne Hu, Rennan Barkana, and Andrei Gruzinov. Cold and fuzzy dark matter. *Phys. Rev. Lett.*, 85:1158–1161, 2000.

[10] P. Sikivie and Q. Yang. Bose-Einstein Condensation of Dark Matter Axions. *Phys. Rev. Lett.*, 103:111301, 2009.

[11] Lam Hui, Jeremiah P. Ostriker, Scott Tremaine, and Edward Witten. Ultralight scalars as cosmological dark matter. *Phys. Rev.*, D95(4):043541, 2017.

[12] Lasha Berezhiani and Justin Khoury. Theory of dark matter superfluidity. *Phys. Rev.*, D92:103510, 2015.

[13] Elisa G. M. Ferreira, Guilherme Franzmann, Justin Khoury, and Robert Brandenberger. Unified Superfluid Dark Sector. 2018.

[14] Stephon Alexander and Sam Cormack. Gravitationally bound BCS state as dark matter. *JCAP*, 1704(04):005, 2017.

[15] Stephon Alexander, Evan McDonough, and David N. Spergel. Chiral Gravitational Waves and Baryon Superfluid Dark Matter. *JCAP*, 1805(05):003, 2018.

[16] T. Rindler-Daller, P.R. Shapiro. Angular momentum and vortex formation in Bose-Einstein-condensed cold dark matter haloes. *MNRAS*, 422:135–161, 2012. arXiv.

[17] Robert H. Brandenberger. Topological defects and structure formation. *Int. J. Mod. Phys.*, A9:2117–2190, 1994.

[18] Robert H. Brandenberger. Searching for Cosmic Strings in New Observational Windows. *Nucl. Phys. Proc. Suppl.*, 246-247:45–57, 2014.

[19] S. Mao and P. Schneider. Evidence for Substructure in lens galaxies. *MNRAS*, 295:587–594, 1998. arXiv.

[20] J.W. Hsueh et al. SHARP - IV. An apparent flux ratio anomaly resolved by the edge-on disc in B0712+472. *MNRAS*, 469(3):3713–3721, 2017. arXiv.

[21] N. Dalal and C.S. Kochanek. Direct Detection of CDM Substructure. *ApJ*, 572:25–33, 2002. arXiv.

[22] Y.D. Hezaveh et al. Detection of Lensing Substructure Using ALMA Observations of the Dusty Galaxy SDP.81. *ApJ*, 823(1):37–56, 2016. arXiv.

[23] S. Vegetti and L.V.E. Koopmans. Bayesian strong gravitational-lens modelling on adaptive grids: objective detection of mass substructure in Galaxies. *MNRAS*, 392(3):945–963, 2009. arXiv.

[24] L.V.E. Koopmans. Gravitational imaging of cold dark matter substructures. *MNRAS*, 363(4):1136–1144, 2005. Oxford Journals.

[25] S. Vegetti and L.V.E. Koopmans. Statistics of mass substructure from strong gravitational lensing: quantifying the mass fraction and mass function. *MNRAS*, 400:1583–1592, 2009. arXiv.

[26] G Kauffmann, Simon D. M. White, and B. Guiderdoni. The Formation and Evolution of Galaxies Within Merging Dark Matter Haloes. *Mon. Not. Roy. Astron. Soc.*, 264:201, 1993.

[27] T. Rindler-Daller, P. R. Shapiro. Angular Momentum and Vortex Formation in Bose-Einstein-Condensed Cold Dark Matter Haloes. *MNRAS*, 422(1):135–161, 2012. arXiv:1106.1256.

[28] A. Verma, T. Collett et al. Strong Lensing considerations for the LSST observing strategy. 2019. arXiv.

[29] J.W. Nightingale and S. Dye. Adaptive semi-linear inversion of strong gravitational lens imaging. *MNRAS*, 452(3):2940–2959, 2015. arXiv.

[30] J.W. Nightingale, S. Dye, and R.J. Massey. AutoLens: automated modeling of a strong lens's light, mass, and source. *MNRAS*, 478(4):4738–4784, 2018. arXiv.

[31] T. Daylan et al. Probing the Small-scale Structure in Strongly Lensed Systems via Transdimensional Inference . *ApJ*, 854(2):141–163, 2018. arXiv.

[32] Kaiming He, Xiangyu Zhang, Shaoqing Ren, and Jian Sun. Deep residual learning for image recognition. *CoRR*, abs/1512.03385, 2015.

[33] Alex Krizhevsky, Ilya Sutskever, and Geoffrey E. Hinton. Imagenet classification with deep convolutional neural networks. *Commun. ACM*, 60(6):84–90, May 2017.

[34] Gao Huang, Zhuang Liu, and Kilian Q. Weinberger. Densely connected convolutional networks. *CoRR*, abs/1608.06993, 2016.

[35] Karen Simonyan and Andrew Zisserman. Very Deep Convolutional Networks for Large-Scale Image Recognition. *arXiv e-prints*, page arXiv:1409.1556, Sep 2014.